Soft-Clamped Silicon Nitride String Resonators at Millikelvin Temperatures

Originally published in:
Physical Review Letters 129(10), https://doi.org/10.1103/PhysRevLett.129.104301

Funding acknowledgement:
ETH-51 19-2 - Differential magnetic imaging with an inverted scanning force microscope (ETHZ)
177198 - Zeptonewton force sensing on a membrane resonator platform (SNF)

Supplemental Material for:
Soft-clamped silicon nitride string resonators at millikelvin temperatures

Thomas Gisler,[1] Mohamed Helal,[1] Deividas Sabonis,[1] Urs Grob,[1] Martin Héritier,[1] Christian L. Degen,[1] Amir H. Ghadimi,[2,*] and Alexander Eichler[1,†]

[1] *Laboratory for Solid State Physics, ETH Zürich, 8093 Zürich, Switzerland.*
[2] *Centre Suisse d'Electronique et de Microtechnique SA (CSEM), 2002 Neuchâtel, Switzerland.*

S1. OPTICAL FRINGES

Tuning the wavelength by changing the temperature of the laser diode allows to move within the optical fringe. For this we apply a voltage to the thermoelectric cooler (TEC) pins of the butterfly laser diode. While the motion of the string is encoded in the interference of the light reflected from the string resonator and the coated fiber end, the main fraction of the reflected light comes from the sample chip substrate, see Fig. S1(a). This results in the optical fringe shown in Fig. S1(b). Using a phase-lock loop (PLL) to drive and measure the displacement of the fundamental mode of the string - while sweeping the TEC voltage - reveals the position within the fringe where the largest signal is obtained. The TEC voltage sweep is performed for two different PLL setpoint phases shifted by π (orange and green in Fig. S1(b)). The mechanical signal is not maximized at the steepest slope of the optical fringe, as is typically observed with this interferometer setup [1]. Instead, the maximum position cannot be predicted from the fringe signal and must be measured directly as a function of the TEC voltage, as described above. The laser wavelength is then locked to this point using a PID feedback. This point corresponds to where the phase light reflected from the fiber end and the string are shifted by $\pm\pi$. The maxima of the orange and green signals correspond to maximum positive and negative optomechanical damping, respectively.

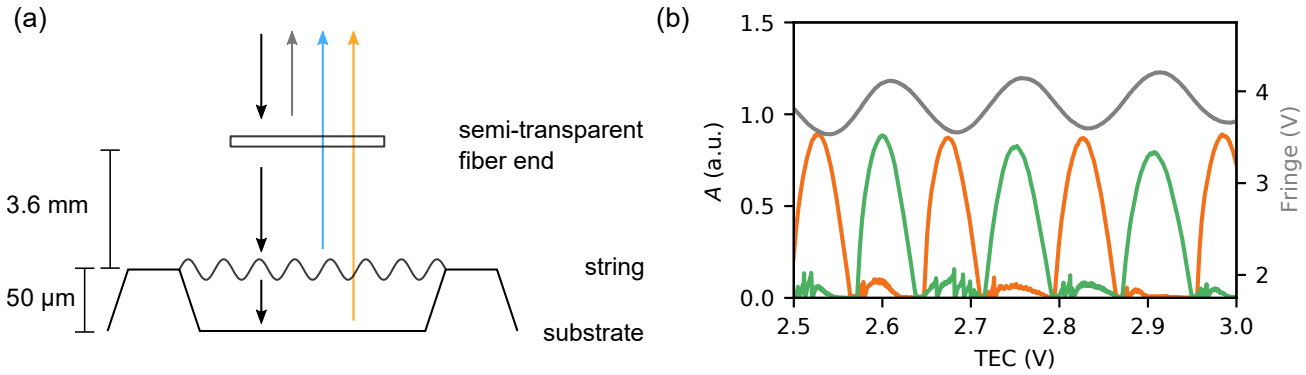

FIG. S1. **Interferometric detection method.** (a) Schematic of the optical interferometer, with light reflected from the fiber end (grey), the string (blue) and the substrate (orange). (b) Sweeping the TEC voltage (corresponds to laser wavelength) and measuring the optical fringe (grey - right y-axis) and the amplitude of the fundamental mode with two different PLL setpoint phases ϕ_{PLL} (orange: $\phi_{\mathrm{PLL}} = \phi_0$, green: $\phi_{\mathrm{PLL}} = \phi_0 + \pi$, left y-axis).

* Corresponding author: amir.ghadimi@csem.ch
† Corresponding author: eichlera@ethz.ch

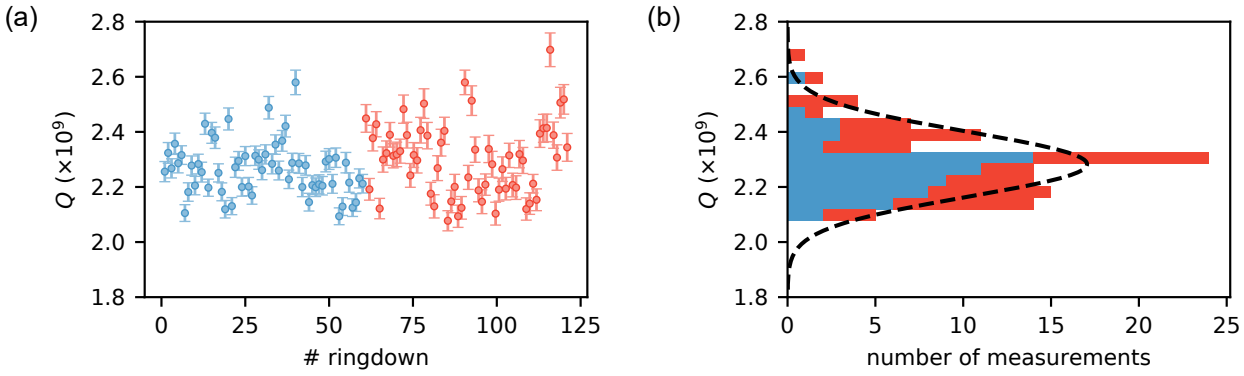

FIG. S2. **Repeatability of measured Q.** Repetition of ringdown measurements with $t_{\mathrm{on}} = 5\,\mathrm{s}$ for two different "laser off" periods ($t_{\mathrm{off}}^{\mathrm{blue}} = 150\,\mathrm{s}$ and $t_{\mathrm{off}}^{\mathrm{red}} = 250\,\mathrm{s}$). (a) Measured Q and (b) histogram of these values together with a Gaussian fit with mean value 2.282×10^9 and standard deviation 0.116×10^9.

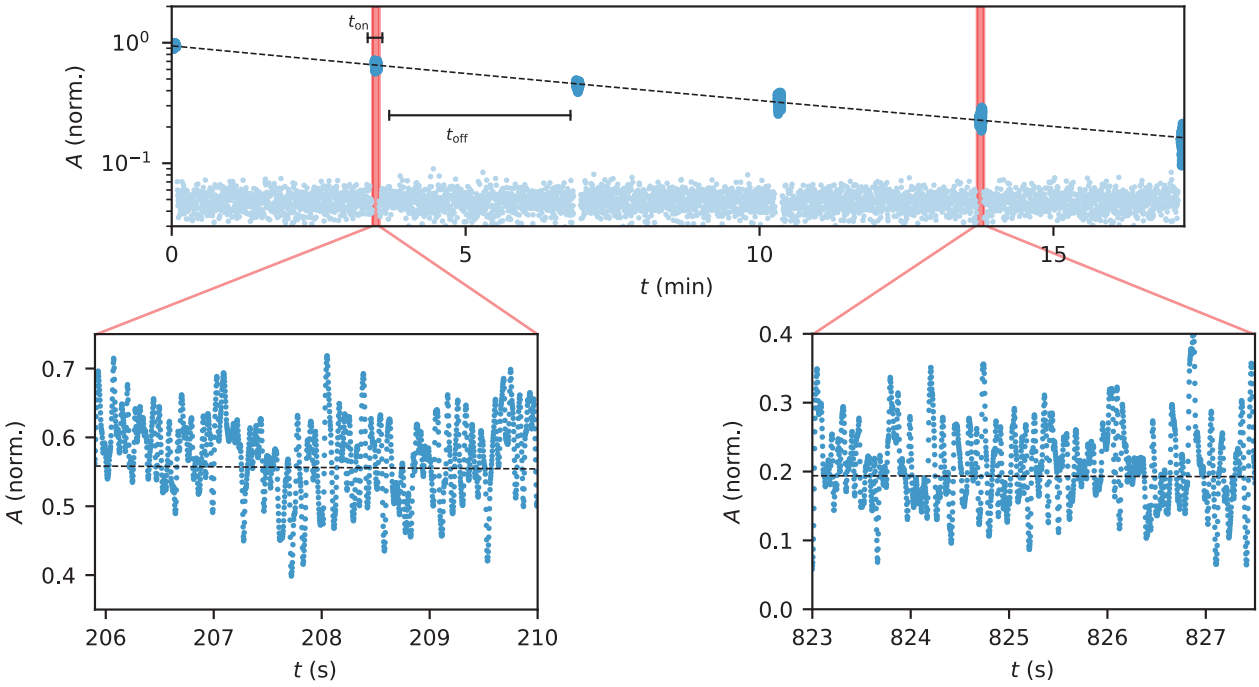

FIG. S3. **Zoom ringdown** The same ringdown as in Fig. 1(c) presented with zoomed details. The large spread of data points is due to detector noise.

S2. REPEATABILITY OF RINGDOWN MEASUREMENTS

In order to verify the measured Q we repeatedly conducted ringdown measurements with the same settings. In Fig. S2(a-b) we collect the extracted Q values of the localized mode for $t_{\mathrm{off}} = 150\,\mathrm{s}$ and $250\,\mathrm{s}$ of device B at $T_{plate} = 48\,\mathrm{mK}$ and $t_{\mathrm{on}} = 5\,\mathrm{s}$. The mean of the measured values is 2.282×10^9 with a standard deviation of 0.116×10^9. This mean value for Q is used to calculate the intrinsic force sensitivity and thermal decoherence time in the main text. The zoomed data in Fig. S3 demonstrate the large spread of data points due to the low-pass filtered detector noise.

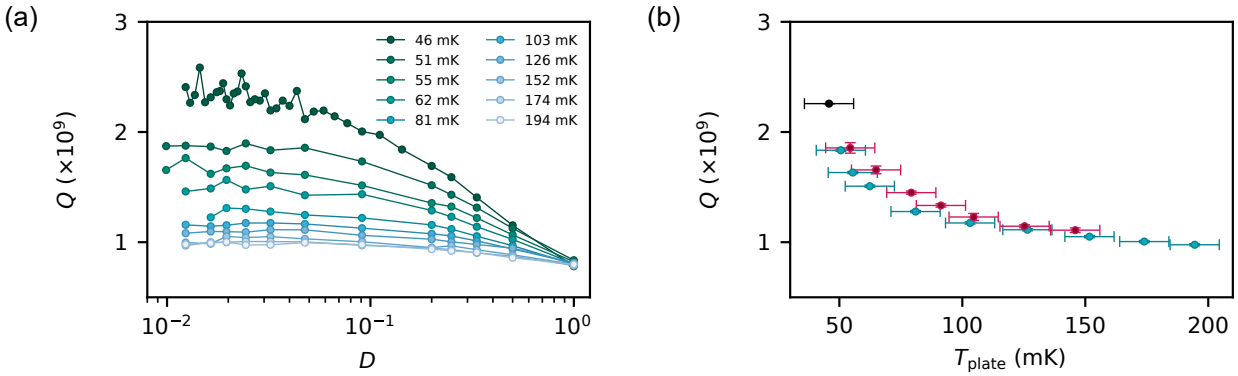

FIG. S4. **Comparing the different heaters.** (a) Driven PEA with frequency 1.5 MHz with driving amplitudes between 50 mV and 200 mV. The temperatures in the legend correspond to T_{plate}. Note that the top line, corresponding to the unheated string, is identical to the measurement in the main text. (b) Comparison of Q as a function of T_{plate} for the two heaters (blue closer to the sample than purple).

S3. VARIABLE TEMPERATURE MEASUREMENTS

We used two different heaters to locally change the temperature of the nanomechanical resonator. For each temperature T_{plate} (extracted from the mixing chamber temperature, see Fig. S5) we extracted Q for different duty cycles D. In the main text, data are shown for a resistive heater mounted a few centimeters from the sample on the sample plate. In Fig. S4(a) we supply the results for the second heater, consisting of the piezoelectric actuator (PEA) mounted closer to the string chip. Here, a temperature variation was induced by applying a high-frequency signal $f_{\mathrm{heat}} = 1.5\,\mathrm{MHz}$ to the PEA, carefully avoiding any mechanical resonance frequency. In Fig. S4(b) we compare the results of the two heating methods and obtain very similar Q values.

S4. CALIBRATION OF SAMPLE PLATE TEMPERATURE

During the measurements presented in the main text, the thermometer mounted on the sample plate could not be used due to a wiring problem. We later repeated the cooldown (without a mechanical resonator device) to calibrate the temperature difference between the mixing chamber plate and the sample plate. All temperatures in the main text are stated after the conversion using the calibration measurement shown in Fig. S5. We infer a base temperature of 41 mK on the sample plate with a systematic uncertainty of 10 mK stemming from the sensor calibration. The measurement was performed with a lock-in amplifier at a bias current of roughly 1 nA applied with a local oscillator frequency of 33 Hz. The power dissipated over the temperature sensor was below 1 pW.

S5. SILICON NITRIDE STRINGS

A. Fabrication

The devices used in this work were designed and fabricated at CSEM based on the previous work by authors [2, 3]. Briefly, the fabrication process flow starts with a low-pressure chemical vapor deposition (LPCVD) of high-stress

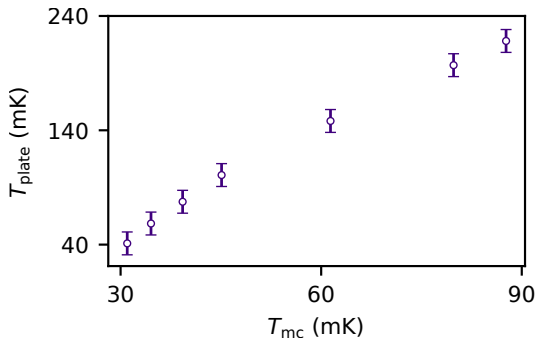

FIG. S5. **Calibration of sample plate temperature.** Sample plate temperature T_{plate} as function of the mixing chamber temperature T_{mc} for variable power delivered to a heater on the sample plate. The error bars correspond to the calibration uncertainty (10 mK) of the RuO_2 sensor.

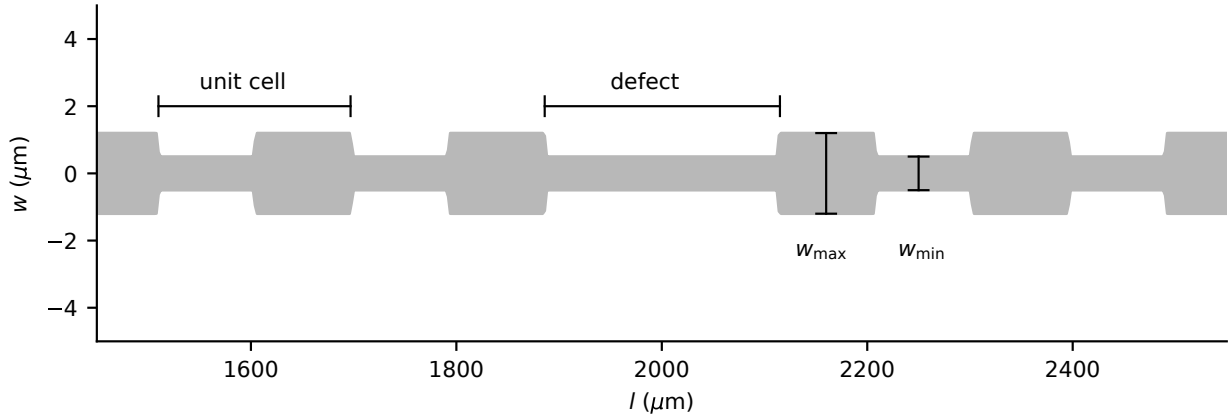

FIG. S6. **Nanostring geometry.** Geometrical shape of the silicon nitride string with $w_{\mathrm{min}} = 500\,\mathrm{nm}$ and $w_{\mathrm{max}} = 1200\,\mathrm{nm}$ and a length of 4 mm.

Si_3N_4 on a Si substrate. This is followed by electron beam (ebeam) lithography of the corrugated string geometry on top of Si_3N_4 layer using a flowable oxide (FOX-16 ®) resist (2). Structures are then transferred to the Si_3N_4 layer by reactive ion etching (RIE). Finally, the mechanical beams are released from the underlying Si substrate in potassium hydroxide (KOH) bath and drying using a critical point dryer (CPD). The complete process flow is considerably more complex and includes several intermediate steps to ensure the prevention of collapsing of released nanobeams due to their extreme aspect ratios. The detailed process flow can be found in [2, 3].

B. Geometrical shape of strings

In this work, we used different corrugated Si_3N_4 strings with similar geometries. Figure S6 shows the area around the defect in the center of such a string. Device B and C have the same thickness, size and number of unit cell but their defect-to-unit-cell ratio differs (Device B 1.1 and device C 1.2).

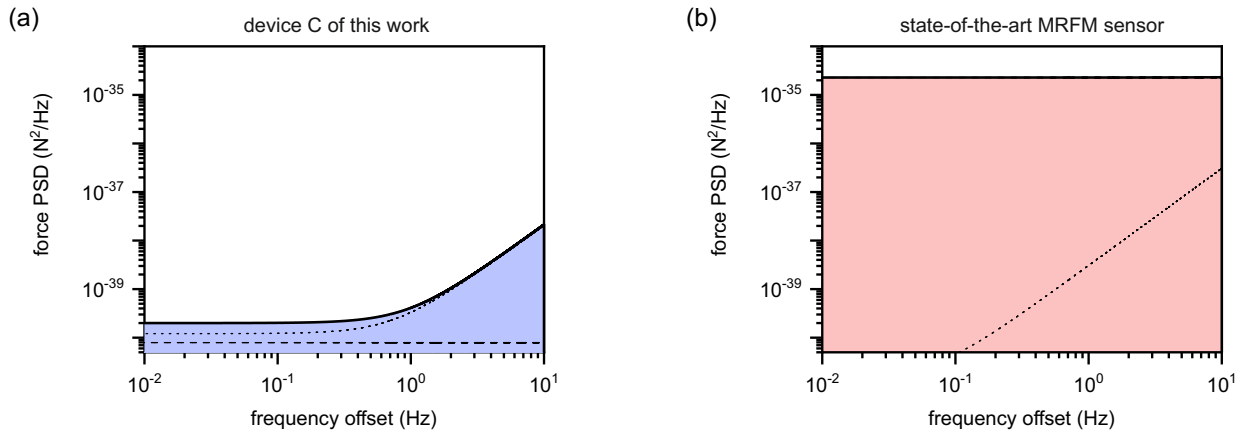

FIG. S7. **Force sensitivity comparison as a function of the detuning from the resonance frequency f_0.** (a) Estimated contributions to the force noise power spectral density of device C measured in this work at a conservative temperature of 80 mK. We assume that an on-chip cavity readout can reach a displacement sensitivity of $2 \times 10^{-28}\,\mathrm{m^2\,Hz^{-1}}$ without significant additional heating [6, 7]. For the magnetic field gradient produced by a coated AFM tip at a distance of 10 to 30 nm, we use a conservative value of $1 \times 10^{7}\,\mathrm{T\,m^{-1}}$. (b) Cantilever device used in state-of-the-art NanoMRI measurements with a mass of 1×10^{-13} pg, a resonance frequency of 3.5 kHz and a quality factor of 25000, (manuscript in preparation, similar performance as in Ref. [5]). This sensor is operated at 4.7 K and no on-chip cavity readout is possible in the present setup, limiting the displacement sensitivity to $4 \times 10^{-24}\,\mathrm{m^2\,Hz^{-1}}$. The magnetic field gradient produced by the nanomagnet in this experiment was found to have a maximum value of $2.8 \times 10^{6}\,\mathrm{T\,m^{-1}}$. In both panels, a dashed black line is the thermal noise (including the zero-point fluctuations), a dotted black line is the sum of quantum back-action and detector noise, and a thick black line and the colored area indicate the total force noise. The noise of the cantilever device in (b) is dominated by the thermomechanical noise contribution, such that the solid and dashed black lines overlap.

C. Force noise evaluation for nanoscale MRI

The devices used in this work are promising candidates for force sensing in the zeptonewton range. Such a force sensitivity is crucial, for instance, for nanoscale magnetic resonance microscopy (NanoMRI) and for coherent spin-mechanics coupling. In Fig. S7, we compare the predicted performance of device C measured in this work with a state-of-the-art cantilever sensor used for our most recent NanoMRI demonstration [4], which is comparable to that used in previous experiments [5]. The only modification that we additionally assume for the string device in Fig. S7(a) is the implementation of an on-chip cavity readout with a displacement sensitivity of $2 \times 10^{-28}\,\mathrm{m^2\,Hz^{-1}}$, as discussed in the main text [6, 7]. For a bandwidth of 1 Hz, the present string device has a total force noise standard deviation of 1.7×10^{-20} N, corresponding to the force generated by 0.0.1 hydrogen atoms in the magnetic field gradient predicted from finite element calculations. The cantilever device in Fig. S7(b) achieves a force noise standard deviation of 3.4×10^{-18} N in the same bandwidth, resulting in a theoretical sensitivity of roughly 7400 hydrogen atoms. The string resonator is therefore expected to produce highly superior results, allowing the detection of the forces generated by individual nuclei.

[1] M. Héritier, A. Eichler, Y. Pan, U. Grob, I. Shorubalko, M. D. Krass, Y. Tao, and C. L. Degen, Nanoladder cantilevers made from diamond and silicon, Nano Letters **18**, 1814 (2018).

[2] A. H. Ghadimi, S. A. Fedorov, N. J. Engelsen, M. J. Bereyhi, R. Schilling, D. J. Wilson, and T. J. Kippenberg, Elastic strain engineering for ultralow mechanical dissipation, Science **360**, 764 (2018).

[3] A. H. Ghadimi, *Ultra-coherent nano-mechanical resonators for quantum optomechanics at room temperature*, Tech. Rep. (EPFL, 2018).

[4] M.-D. Krass, N. Prumbaum, R. Pachlatko, U. Grob, H. Takahashi, Y. Yamauchi, C. L. Degen, and A. Eichler, Force-detected magnetic resonance imaging of influenza viruses in the overcoupled sensor regime, arXiv preprint arXiv:2206.03168 (2022).

[5] U. Grob, M.-D. Krass, M. Héritier, R. Pachlatko, J. Rhensius, J. Košata, B. A. J. Moores, H. Takahashi, A. Eichler, and C. L. Degen, Magnetic resonance force microscopy with a one-dimensional resolution of 0.9 nanometers, Nano Lett. **19**, 7935 (2019).

[6] R. Schilling, H. Schütz, A. H. Ghadimi, V. Sudhir, D. J. Wilson, and T. J. Kippenberg, Near-field integration of a SiN nanobeam and a SiO_2 microcavity for Heisenberg-limited displacement sensing, Phys. Rev. Applied **5**, 054019 (2016).

[7] J. Guo, R. Norte, and S. Gröblacher, Feedback cooling of a room temperature mechanical oscillator close to its motional ground state, Phys. Rev. Lett. **123**, 223602 (2019).